NANOSYSTEMS: PHYSICS, CHEMISTRY, MATHEMATICS, 2019, 10 (4), P. 428–437

The minimum size of oxide nanocrystals: phenomenological thermodynamic vs crystal-chemical approaches

O. V. Almjasheva[1,2], N. A. Lomanova[2], V. I. Popkov[2], O. V. Proskurina[2,3], E. A. Tugova[2], V. V. Gusarov[2]

[1]Saint Petersburg Electrotechnical University "LETI", St. Petersburg, 197376 Russia
[2]Ioffe Institute, Politekhnicheskaya St. 26, St. Petersburg, 194021, Russia
[3]St. Petersburg State Institute of Technology, Moskovsky Pr., 26, St. Petersburg, 190013, Russia

almjasheva@mail.ru, nat-lomanova@yandex.ru, vadim.i.popkov@technolog.edu.ru, proskurinaov@mail.ru, katugova@inbox.ru, victor.v.gusarov@gmail.com

PACS 61.46.+w, 64.60.Qb **DOI 10.17586/2220-8054-2019-10-4-428-437**

The minimum crystallite size in a group of oxides has been analyzed as a function of their synthesis conditions, critical nucleus size and the crystal structure parameters. Nanocrystals were synthesized by solution combustion, hydrothermal synthesis and heat treatment in air of the precipitated hydroxides. Aluminum and iron oxides, titania and zirconia, cobalt ferrite, $AFeO_3$ ferrites (A = Bi, RE), Aurivillius phases $Bi_{m+1}Ti_3Fe_{m-3}O_{3m+3}$ ($m = 3 - 9$), as well as solid solutions based on these phases were chosen as the objects of the study. The presence of a correlation between the crystalline oxide unit cell parameters and the synthesized crystals minimum size is shown. A conclusion was made about the impossibility to use only the thermodynamic concept of the critical nucleus for determining the minimum possible particle size of a new phase in some cases of oxide nanocrystals synthesis. The paper demonstrates a necessity to use crystal-chemical criteria that complement the methods of phenomenological thermodynamics and kinetics for determining the minimum possible particle size of the resulting crystalline oxide phases synthesized under the considered conditions.

Keywords: nucleation, nanocrystals, oxides, crystal structure, soft chemistry, solution combustion.

Received: 3 December 2018

Revised: 1 August 2019

1. Introduction

Though the methods based on phenomenological thermodynamics and on macrokinetic models of phase formation processes [1–22] are widely used for determining the minimum limit size of crystallites [1–22], these approaches encounter a series of problems when describing the formation of nanocrystals. Some possibilities to expand these methods are based on determining how thermodynamic model parameters, in particular, the specific surface energy, depend on particle size [23–30]. Another possibility is to describe the features of nucleation taking into account the presence in the reaction system of the variously shaped and sized subcritical clusters, which determine the high rate of stable nanoparticles formation in a new phase [10,31–48]. However, these approaches do not solve all the problems of describing nucleation processes in the case of a crystalline phase formation. For example, at certain ratios of specific surface energy values for the new phase particles and the Gibbs energy of their formation, cases are possible when the calculated size of the crystal critical nucleus is smaller or comparable with the size of its unit cell. Such cases are presented, e.g., in [47]. Since the unit cell of a crystal is its minimum structural element, the translation of which builds a crystalline particle, the above hypothetical cases cannot exist in reality, as the very principle of a crystalline body formation will be violated. Consequently, the minimum size of the forming particles in the case of crystallite formation should be determined not only by the thermodynamically-determined critical nuclei size, but also by other reasons. For example, the minimum size of crystals may be related to the dependence of the crystal structure stability on the number of the minimum building blocks in the crystal lattice, i.e., on the elementary cells that form the crystalline particles, and also, apparently, on the crystalline particles morphology, and on the unit cell composition and structure. Experimental determination of the crystalline particles minimum size dependence on these factors is complicated by a number of issues. First of all, it is not always possible to calculate the values of the critical nucleus size for particular phase formation conditions. This means that it is impossible to attribute the experimentally-obtained dimensions of the synthesized crystal particles to a factor associated with the nucleation process, or to a factor determined by the dependence of the forming phase crystalline structure stability on the number of unit cells contained by this crystalline particle, and on their crystal-chemical features. On the other hand, as a rule, it is very difficult to experimentally register the minimum possible values of the crystalline particle size due to the rapid growth of nanoscale crystals during phase formation [49–52], which depends on the conditions of their synthesis [38, 42, 43, 46, 52–59]. Crystal growth can be reduced by using special synthetic methods, which include, in particular, soft chemistry methods,

when synthesis proceeds at relatively low temperatures [36–48, 52–59]. Another group of methods that includes, for example, solution combustion, self-propagating high-temperature synthesis (SHS), autocatalytic and other fast solid-state reactions, is based on the use of rapid synthesis [49–51, 60–71]. Crystal growth can often be restricted by using nano- and microreactors, or synthesis methods that use spatial constraints [63, 64, 72–82].

The interest in determining the minimum possible size of crystals is determined by the possibility of creating promising functional and structural nanomaterials based on such crystalline particles [83–87]. One such widely used class of nanomaterials is represented by oxide nanocrystalline materials [35–58, 83–87]. At the same time, literature offers no systematic analysis of the influence of chemical composition, features of the crystal structure, and of the methods and conditions of the nanocrystals synthesis on the possible limit values of their size.

The listed reasons show the relevance for the problem of determining the effect of methods and synthetic conditions, and of thermodynamic and crystal-chemical characteristics on the production of oxide nanocrystals with the smallest possible size.

2. Methods

2.1. Calculations and modeling

The sizes of critical nuclei were calculated for the methods of solid phase synthesis that were used in the work, and for the cases when it was possible to obtain information on the specific surface energy of the particles and on thermodynamic properties of the phases required for calculating the Gibbs energy of the corresponding reactions. The data for thermodynamic properties of the phases were taken mainly from the databases listing the thermodynamic properties of substances [88, 89]. In some cases, when the necessary experimental information was missing, approximate methods of modeling and calculating thermodynamic properties were used. The use of such calculations is described in [47]. In order to compare the experimental and calculated data, the critical nuclei sizes were calculated for the phase formation conditions identical to the actual conditions of nanocrystals synthesis.

2.2. Experiment

Nanocrystalline oxide particles were synthesized by three main methods, which make it possible to use the data from [33, 35–48, 60–69, 90, 91] and obtain nanocrystals of relatively small size and narrow size distribution. The methods of precipitated hydroxides decomposition under hydrothermal conditions and thermal treatment in air were used as soft chemistry methods for synthesizing oxide nanocrystals. The other method for synthesizing oxide nanocrystals was solution combustion. The conditions of nanoparticle synthesis by these methods have been previously described [33, 35–48, 63–66, 77–80, 92–94]. In some cases, the growth of nanocrystals was retarded by applying techniques based on the organization and self-organization of spatial constraints that prevent mass transfer and, consequently, the growth of nanocrystals during the synthesis [63, 72, 77–80].

Crystal sizes in the synthesized phases were determined mainly using the data on the width of the X-ray diffraction lines. The calculations were carried out mainly using the Scherrer formula and assuming the isometric form of crystallites and narrow crystallite size distribution. The possibility of using such calculations for determining the size of crystallites in the considered cases was based on the coincidence of the crystal size data obtained by different methods when analyzing a number of oxide nanocrystals synthesized under the conditions similar to the considered ones [77, 79, 95].

3. Results and discussion

Table 1 presents the calculated values of the critical nucleus size (d_{cr}) of some oxides for different conditions of their formation. The maximum values of the unit cells parameters ($L_{\max}$) of these crystalline phases are given for comparison.

It should be noted that under the considered nucleation conditions, d_{cr} exceed $L_{\max}$ by almost 10-fold for the phases based on zirconia, α-Al_2O_3 and γ-Al_2O_3, while for other compounds, this difference is less significant. For example, in some cases of Cr_2O_3 formation, d_{cr} exceeds $L_{\max}$ only by 2-4-fold. The d_{cr} values calculated for some conditions of α-Fe_2O_3, γ-Fe_2O_3, and TiO_2 (rutile) formation are comparable with those of $L_{\max}$. This result raises great doubts about the legitimacy of using the thermodynamic approach for estimating the minimum values of the dimensions of a stable crystalline phase, since it is impossible to imagine a crystalline phase consisting of a single unit cell. The calculation of d_{cr} for the TiO_2 (anatase) formation yields a result that is absolutely unrealistic for crystalline phases. In this case, $d_{cr} < L_{\max}$ (see Table 1), but the size of a crystalline particle cannot be smaller than the minimum translation unit that forms the crystal, which is the unit cell of the crystal. An analysis of the performed calculations of the critical nucleus size showed that in the case of crystalline phases, the d_{cr} value cannot be regarded as an estimate of the minimum possible size of the forming nanocrystal.

TABLE 1. Calculated values of the critical nucleus size depending on the synthesis conditions

Substance	$L_{\max}$, **nm**	d_{cr}, **nm**	**Synthesis conditions**	
			Initial substance	T,°C / P, **atm**
m-ZrO_2	0.531 [PDF 01-089-9066]	5 – 9 – 40	Amorphous $ZrO(OH)_2$	250 / 1 – 100 – 600
		5 – 10		300 – 200 / 700
t-ZrO_2	0.527 [PDF 00-042-1164]	5 – 12 – 35		250 / 1 – 100 – 300
		8 – 30		300 – 200 / 700
c-ZrO_2	0.509 [PDF 01-072-2742]	8 – 45		250 / 1 – 100
		10 – 40		300 – 200 / 700
TiO_2-rutile	0.459 [PDF 01-089-4202]	0.44 – 0.65 – 0.8	Amorphous $TiO_2 \cdot nH_2O$	375 – 120 – 25 / 1
		0.46 – 1.0 – 0.85		575 – 120 – 25 / 1000
TiO_2-anatase	0.951 [PDF 01-089-4203]	0.5 – 0.6		120 – 25 / 1
		0.6 – 0.75		120 – 25 / 1000
α-Al_2O_3	1.299 [PDF 01-089-7717]	8 – 40	γ-AlOOH	300 – 200 / 20
		5 – 35		500 – 300 / 700
		18 – 50	α-AlOOH	500 – 450 / 20
		30 – 75		500 – 475 / 700
γ-Al_2O_3	0.794 [PDF 01-076-4179]	5 – 40	γ-AlOOH	500 – 300 / 20
		10 – 40		500 – 400 / 700
		10 – 55	α-AlOOH	450 – 350 / 20
α-Fe_2O_3	1.375 [PDF 01-087-1166]	1 – 25	γ-FeOOH	500 – 100 / 1
		2.5 – 15		500 – 250 / 100
γ-Fe_2O_3	2.501 [PDF 00-013-0458]	2 – 25		500 – 200 / 1
		3 – 15		600 – 400 / 100
Cr_2O_3	1.359 [PDF 01-082-1484]	3 – 10	γ-CrOOH	750 – 550 / 1
		5 – 20		850 – 750 / 100

Table 2 presents the experimentally determined sizes (d) of oxide nanocrystals synthesized under different conditions. An analysis of the data in Table 2 shows that $d \gg L_{\max}$ for all the considered methods of synthesis.

Table 2: Nanocrystal sizes in some simple and complex oxides

Composition	$\boldsymbol{L_{\max}}$**, nm**	$\boldsymbol{d}$**, nm**
m-ZrO_2	0.531 [PDF 01-089-9066]	15–25*
t-ZrO_2	0.527 [PDF 00-042-1164]	10–30*; 5-10*
c-ZrO_2	0.509 [PDF 01-072-2742]	4–20*(solid solutions with Y_2O_3)
TiO_2-rutile	0.459 [PDF 01-089-4202]	∼4 [96]; ∼30 [97]; ∼10*; 68–80 [98]
TiO_2-anatase	0.951 [PDF 01-089-4203]	7–45*; 5–12 [99]; 10–50 [100]; 10–20 [101],5–10*; 20–27 [98]
TiO_2-brookite	0.918 [PDF 03-065-2448]	∼10*; ∼50 [102]; ∼20 [103]
α-CeO_2	0.539 [PDF 01-073-6318]	6–31 [104]; 6–8 [105]
α-Al_2O_3	1.299 [PDF 01-089-7717]	60–100*, 10 [106]
γ-Al_2O_3	0.794 [PDF 01-076-4179]	16–13 [107]
η-Al_2O_3	0.791[ICSD 28260]	5 [108]
α-Fe_2O_3	1.375 [PDF 01-087-1166]	∼30 (160°C, 15 MPa, 2 h.); 11–32 [104]; 13–14 [105]; 57 [109, 110]; 27–30 [41]
γ-Fe_2O_3	2.501 [PDF 00-013-0458]	6-8 [111]
Cr_2O_3	1.359 [PDF 01-082-1484]	25*
α-Y_2O_3	1.061 [PDF 01-089-5591]	18–20 [41]
$CoFe_2O_4$	0.839 [PDF 01-078-4451]	6–50*; 7–15*; ∼10*
$BiFeO_3$	1.388 [PDF 01-077-9630]	20*(450°C); ∼100*(850°C); 71–72*(550°C); 21–70 [112]; 23 [113]; 26 [113]; 41–75 [114] ; 38 [115] ; 17 [77]
$NdFeO_3$	0.776 [PDF 01-089-6644]	7*; 20*; 40*;75 [116]; 20 [117]; 45 – 75 [118]; 42 [119]; 50 (TEM), 36.8 (XRD) [120]; 88 [121]; 50 [122]; 30–50 [123]; 42±1(XRD), 44±1 (SEM) [124]; 35-45 (HRTEM), 12 (XRD) [125]
o-$YFeO_3$	0.760 [PDF 01-089-2609]	50–70 [41]; 30–52 [126, 127]; 25–35 [45, 128]; 17–40 [65]
o-$LaFeO_3$	0.785 [PDF 01-076-7897]	16–37 [129]
o-$GdFeO_3$	0.768 [PDF 00-047-0067]	18–36 [129]; 21–48 [130]
o-$CeFeO_3$	0.781 [PDF 00-022-0166]	32–51 [104]
o-$EuFeO_3$	0.769 [PDF 01-074-1475]	28–46 [132]
o-$HoFeO_3$	0.761 [PDF 00-046-0115]	20–40 [132]

Continued on next page

Table 2: continued from previous page

Composition	$L_{\max}$, nm	d, nm
h-$YFeO_3$	1.172 [PDF 00-048-0529]	6–11 [63, 64]; 5–8 [65]
h-$HoFeO_3$	1.172*	5–10*
$Bi_{1-x}Ca_xFeO_{3-\delta}$ ($x = 0.1$–0.56)	—	20–40*(550°C)
$Bi_{1-x}Sr_xFeO_{3-\delta}$ ($x = 0.1$–0.5)	—	50±2*(550°C)
$Bi_4Ti_3O_{12}$ ($m = 3$)	3.28 [PDF 01-089-7500]	35*(450°C); 60*(800°C); 21 [133]; 20–25 [134], 40–70 [134]; 57 [135]
$Bi_5FeTi_3O_{15}$ ($m = 4$)	4.13 [PDF 00-021-0818]	30*(450°C); 82*(800°C); 18–80 [136]
$Bi_6Fe_2Ti_3O_{18}$ ($m = 5$)	4.9 [PDF 01-075-8378]	36*(450°C); 80*(800°C)
$Bi_7Fe_3Ti_3O_{21}$ ($m = 6$)	5.7 [PDF 01-075-8067]	30*(450°C); 63*(800°C)
$Bi_8Fe_4Ti_3O_{24}$ ($m = 7$)	6.5*	28*(450°C); 57*(800°C)
$Bi_9Fe_5Ti_3O_{27}$ ($m = 8$)	7.6 [PDF 00-021-0100]	30*(450°C); 56*(800°C)
$Bi_{10}Fe_6Ti_3O_{30}$ ($m = 9$)	8.1*	24*(450°C); 54*(800°C)
$Bi_xNd_{1-x}FeO_3$ ($x = 0.2$)	0.778*	30*(600°C)
$Bi_xNd_{1-x}FeO_3$ ($x = 0.4$)	0.779*	40*(600°C)
$Bi_xNd_{1-x}FeO_3$ ($x = 0.6$)	0.781 [PDF 00-061-0719]	50*(600°C)
$Bi_xNd_{1-x}FeO_3$ ($x = 0.7$)	0.783*	50*(600°C)
$Bi_xNd_{1-x}FeO_3$ ($x = 0.75$)	0.784*	40*(600°C)
$Bi_xNd_{1-x}FeO_3$ ($x = 0.8$)	1.118*	40*(600°C)
$Bi_xNd_{1-x}FeO_3$ ($x = 0.85$)	1.266 [48]	23 [137]
$Bi_xNd_{1-x}FeO_3$ ($x = 0.9$)	1.381 [48]	33 [137]
$Bi_xNd_{1-x}FeO_3$ ($x = 0.95$)	1.386 [48]	50 [137]
$Bi_xNd_{1-x}FeO_3$ ($x = 1$)	1.386 [48]	74 [137]
$Bi_xNd_{1-x}FeO_3$ ($x = 0.85$)	0.837 [49]	19 [138]
$Bi_xNd_{1-x}FeO_3$ ($x = 0.9$)	1.182 [49]	19 [138]
$Bi_xNd_{1-x}FeO_3$ ($x = 0.95$)	1.373 [49]	24 [138]
$Bi_xNd_{1-x}FeO_3$ ($x = 1$)	1.383 [49]	25 [138]

Note: *– results of the present work; conditions of nanoparticles synthesis, specifics of their composition or the method for crystal size determination are given in parentheses.

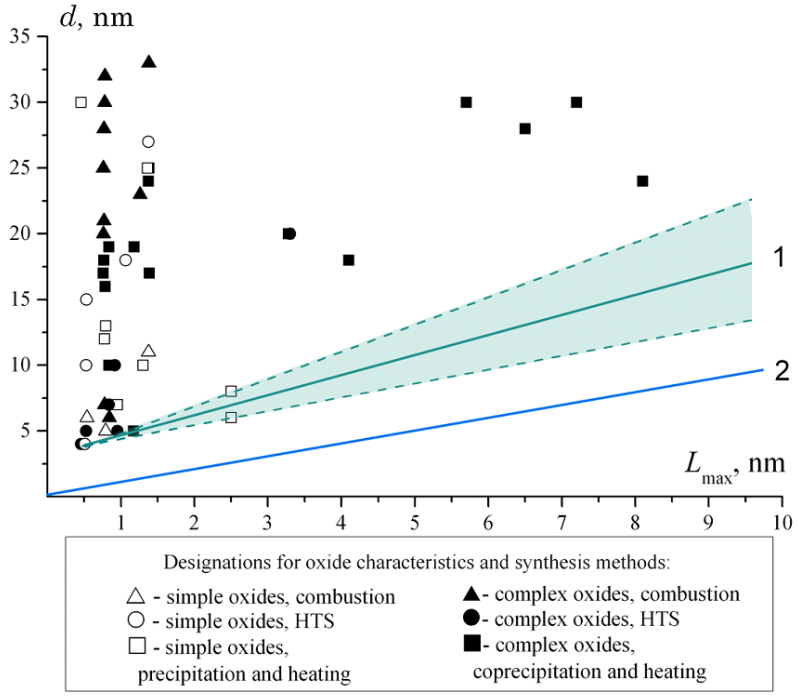

FIG. 1. Dependence of crystallite sizes in synthesized oxide phases (d) on the maximum value of the crystal unit cell parameter ($L_{\max}$) 1 – dependence of the minimum crystal size on the maximum values of the corresponding phase unit cell parameter ($d_{cryst}(L_{\max})$); 2 – $L_{\max} = L_{\max}$ line

The data presented in Fig. 1 show that even the minimal experimentally-obtained values of d (straight line 1) are approximately 3.2 nm above the $L_{\max}$ values (straight line 2).

It should be noted that smaller values of d can more often be achieved in an experiment when synthesizing simple oxides. In this case, the smallest d values for double oxides are observed, as a rule, firstly, when $L_{\max}$ values for these oxides are small, and secondly, when the chosen synthesis conditions limit the mass transfer in the reaction system (see references in Table 2). Mass transfer limitation was achieved either by the synthesis conditions that ensure the presence in the reaction system of structural precursors of the forming crystalline phases and low rates of components diffusion (see, e.g., [37, 45, 77–80]), or by the formation of spatial constraints that inhibit the growth of the formed nanocrystals (see, e.g., [48, 63–65, 72, 139]).

It can be concluded from the data in Table 2 that an increase in the temperature and duration of the synthesis in the absence of spatial limitations in the reaction system leads to a multiple increase in the size of the crystals.

An analysis of experimental and theoretical data demonstrated limitations of the thermodynamic concept of the critical nucleus for estimating the minimum possible size of the synthesized crystalline phases. A comparison of the experimental values of d with the calculated d_{cr} and with the empirical $d_{cryst}(L_{\max})$ dependence shown in Fig. 1 (line 1), allows a conclusion that the minimum size of the synthesized crystals can be determined from the relation:

$$d_{\min} = \max\{d_{cr}, d_{cryst}(L_{\max})\}.$$

The uncertain position of the $d_{cryst}(L_{\max})$ dependence (Fig. 1) seems to be associated with a simplified representation of this dependence as a function of only $L_{\max}$. It can be expected that, depending on the morphology and mechanism of nanocrystals formation, the $d_{\min}$ values will be determined by different parameters of the crystal unit cell. For example, the $d_{\min}$ value may be inconsistent with the proposed dependence in the case of the epitaxial junction of the forming crystal with the crystal matrix. In particular, such cases are possible when the formation of thin layers occurs through the atomic layer deposition (ALD), as was observed in [140].

4. Conclusions

The study has shown that the minimum size of the synthesized crystals can be determined by the critical nucleus size, and also be a function of the crystal unit cell parameters. It is possible to experimentally obtain small size nanocrystals by limiting their growth, which is determined by mass transfer. This can be effectively achieved by

increasing the nucleation rate, or by applying soft chemistry methods for the synthesis, when the process temperature and, therefore, the diffusion rate, are low. Also, it is possible to use synthesis methods, in which spatial constraints (barriers) that form in reaction systems slow down the mass transfer of components to the products of reaction.

Acknowledgements

The present work was supported by the Russian Science Foundation (Project No. 16-13-10252).

References

[1] Tammann G. *Aggregatzustände. Zustandsänderungen der Materie in Abhängikeit von Druck und Temperatur Verlag von Leopold Voss.*, Leipzig, 1922, 237 p.
[2] Volmer M. *Kinetik der Phasenbildung*. T. Steinkopff, Dresden-Leipzig, 1939, 126 p.
[3] Frenkel J. A general theory of heterophase fluctuations and pretransition phenomena. *J. Chem. Phys.*, 1939, **7** (7), P. 538–546.
[4] Zel'dovch Ya. On the theory of new phase formation. Cavitation. *ZhETF*, 1942, **12** (11/12), P. 525–538, (in Russian).
[5] Pound G.M., La Mer V.K. Kinetics of crystalline nucleus formation in supercooled liquid tin. *J. Amer. Chem. Soc.*, 1952, **74**, P. 2323–2332.
[6] Cahn J.W., Hilliard J.E. Free energy of a nonuniform system. III. Nucleation in a two-component incompressible fluid. *J. Chem. Phys.*, 1959, **31** (3), P. 688–700.
[7] Lothe J., Pound G.M. Reconsideration of nucleation theory. *J. Chem. Phys.*, 1962, **36** (8), P. 2080–2085.
[8] Abraham F.F., Pound G.M. Re-examination of homogeneous nucleation theory: statistical thermodynamics aspects. *J. Chem. Phys.*, 1968, **48** (2), P. 732–740.
[9] Reiss H. Treatment of droplike clusters by means of the classical phase integral in nucleation theory. *J. Stat. Phys.*, 1970, **2** (1), P. 83–104.
[10] Kuni F.M., Rusanov A.I. Statistical theory of aggregative equilibrium. *Theor. Math. Phys.*, 1970, **2** (2), P. 192–206.
[11] Blander M., Katz J.L. The thermodynamics of cluster formation in nucleation theory. *J. Stat. Phys.*, 1972, **4** (1), P. 55–59.
[12] Katz J.L., Donohue M.D. A kinetic approach to homogeneous nucleation theory. *Adv. Chem. Phys.*, 1979, **40**, P. 137.
[13] Slezov V.V., Sagalovich V.V. Diffusive decomposition of solid solutions. *Sov. Phys. Usp.*, 1987, **30** (1), P. 23–45.
[14] Ruth V., Hirth J.P., Pound G.M. On the theory of homogeneous nucleation and spinodal decomposition in condensation from the vapor phase. *J. Chem. Phys.*, 1988, **88** (11), P. 7079–7087.
[15] Brener E.A., Marchenko V.I., Formation of nucleation centers in a crystal. *JETP Lett*., 1992, **56** (7), P. 368–372.
[16] Oxtoby D.W. Nucleation of first-order phase transitions. *Acc. Chem. Res.*, 1998, **31** (2), P. 91–97.
[17] Antonov N.M., Popov I.Yu., Gusarov V.V. Model of spinodal decomposition of phases under hyperbolic diffusion. *Phys. Solid State.*, 1999, **41** (5), P. 824–826.
[18] Gorbachev Yu.E., Nikitin I.S. Evolution of cluster size distribution during nucleation with rapidly changing dynamic gas processes. *Tech. Phys.*, 2000, **45** (12), P. 1538–1548.
[19] Oxtoby D.W. Phase transitions: Catching crystals at birth. *Nature*, 2000, **406**, P. 464–465.
[20] Kuni F.M., Shchekin A.K., Grinin A.P. Theory of heterogeneous nucleation for vapor undergoing a gradual metastable state formation. *Phys. Usp.*, 2001, **44** (4), P. 331–370.
[21] Xu D., Johnson W.L. Geometric model for the critical-value problem of nucleation phenomena containing the size effect of nucleating agent. *Phys. Rev. B*, 2005, **72**, P. 052101.
[22] Kukushkin S.A., Osipov A.V. First-order phase transition through an intermediate state. *Phys. Solid State*, 2014, 56 (4), P. 792–800.
[23] Tolman R.C. The effect of droplet size on surface tension. *J. Chem. Phys.*, 1949, **17** (3), P. 333–337.
[24] Rusanov A.I. Phase equilibria and surface phenomena. Khimiya, Leningrad, 1967, 388 p. (in Russian); German edition: Rusanov A.I. Phasengleichgewichte und Grenzflächenerscheinungen. Akademie-Verlag, Berlin, 1978, 465 p.
[25] Bykov T.V., Shchekin A.K. Surface tension, tolman length, and effective rigidity constant in the surface layer of a drop with a large radius of curvature. *Inorganic Materials*, 1999, **35** (6), P. 641–644.
[26] Gordon P.V., Kukushkin S.A., Osipov A.V. Perturbation methods in the kinetics of nanocluster growth. *Phys. Solid State.*, 2002, **44** (11), P. 2175–2180.
[27] Samsonov V.M., Bazulev A.N., Sdobnyakov N.Y. Rusanov's linear formula for the surface tension of small objects. *Doklady Physical Chemistry*, 2003, **389** (1–3), P. 83–85.
[28] Magomedov M.N. Dependence of the surface energy on the size and shape of a nanocrystal. *Phys. Solid State*, 2004, **46** (5), P. 954–968.
[29] Rekhviashvili S.Sh., Kishtikova E.V. On the size dependence of the surface tension. *Tech. Phys.*, 2011, **56** (1), P. 143–146.
[30] Kukushkin S.A., Osipov O.V. New phase formation on solid surfaces and thin film condensation. *Progress in surface science*, 1996, 5 (1), P. 1–107
[31] Kuni F.M., Rusanov A.I. The homogeneous nucleation theory and the fluctuation of the center of mass of a drop. *Phys. Letters. A*, 1969, **29** (6), P. 337–338.
[32] Kligman F.I., Rusanov A.I. On the thermodynamic equilibrium states of disperse systems with suspended particles. *Koll. Zh.*, 1977, **39** (1), P. 44–47. (in Russian)
[33] Pozhidaeva O.V., Korytkova E.N., Drozdova I.A., Gusarov V.V. Phase state and particle size of ultradispersed zirconium dioxide as influenced by condition of hydrothermal synthesis. *Russ. J. General Chem.*, 1999, **69** (8), P. 1219–1222.
[34] Yau S.-T., Vekilov P.G. Quasi-planar nucleus structure in apoferritin crystallization. *Nature*, 2000, **406** (6795), P. 494–497.
[35] Pozhidaeva O.V., Korytkova E.N., Romanov D.P., Gusarov V.V. Formation of ZrO_2 nanocrystals in hydrothermal media of various chemical compositions. *Russ. J. General Chem.*, 2002, **72** (6), P. 849–853.
[36] Sharikov F.Yu., Almjasheva O.V., Gusarov V.V. Thermal analysis of formation of ZrO_2 nanoparticles under hydrothermal conditions. *Russ. J. Inorg. Chem.*, 2006, **51** (10), P. 1538–1542.
[37] Kuznetsova V.A., Almjasheva O.V., Gusarov V.V. Influence of microwave and ultrasonic treatment on the formation of $CoFe_2O_4$ under hydrothermal conditions. *Glass Phys. Chem.*, 2009, **35** (2), P. 205–209.

[38] Krasilin A.A., Almjasheva O.V., Gusarov V.V. Effect of the structure of precursors on the formation of nanotubular magnesium hydrosilicate. *Inorganic Materials*, 2011, **47** (10), P. 1111–1115.
[39] Bugrov A.N., Almjasheva O.V. Formation of Cr_2O_3 nanoparticles under hydrothermal conditions. *Nanosystems: Physics, Chemistry, Mathematics*, 2011, **2** (4), P. 126–132.
[40] Almjasheva O.V., Gusarov V.V. Metastable clusters and aggregative nucleation mechanism. *Nanosystems: Physics, Chemistry, Mathematics*, 2014, **5** (3), P. 405–417.
[41] Popkov V.I., Almjasheva O.V. Formation mechanism of $YFeO_3$ nanoparticles under the hydrothermal condition. *Nanosystems: Physics, Chemistry, Mathematics*, 2014, **5** (5), P. 703–708.
[42] Popkov V.I., Almjasheva O.V., Gusarov V.V. The investigation of the structure control possibility of nanocrystalline yttrium orthoferrite in its synthesis from amorphous powders. *Russ. J. Appl. Chem.*, 2014, 87 (10), P. 1417–1421.
[43] Vasilevskaya A.K., Almjasheva O.V., Gusarov V.V. Formation of nanocrystals in the ZrO_2 –H_2O system. *Russ. J. Gen. Chem.*, 2015, **85** (12), P. 2673–2676.
[44] Almjasheva O.V., Gusarov, V.V. Prenucleation formations in control over synthesis of CoFe2O4 nanocrystalline powders. *Russ. J. Appl. Chem*., 2016, **89** (6), P. 851–856.
[45] Popkov V.I., Almjasheva O.V., et al. The role of pre-nucleus states in formation of nanocrystalline yttrium orthoferrite. *Dokl. Chem.*, 2016, **471** (2), P. 356–359.
[46] Komlev A.A., Panchuk V.V., et al. Effect of the sequence of chemical transformations on the spatial segregation of components and formation of periclase-spinel nanopowders in the MgO–Fe_2O_3–H_2O system. *Russ. J. Appl. Chem*., 2016, **89** (12), P. 1930–1936.
[47] Almjasheva O.V. Formation and structural transformations of nanoparticles in the TiO_2–H_2O system. *Nanosystems: Physics, Chemistry, Mathematics*, 2016, **7** (6), P. 1031–1049.
[48] Almjasheva O.V., Krasilin A.A., Gusarov V.V. Formation mechanism of core-shell nanocrystals obtained via dehydration of coprecipitated hydroxides at hydrothermal conditions. *Nanosystems: Physics, Chemistry, Mathematics*, 2018, **9** (4), P. 568–572.
[49] Gusarov V.V. Fast Solid-Phase Chemical Reactions. *Russ. J. of Gen. Chem.*, 1997, **67** (12), P. 1846–1851.
[50] Gusarov V.V., Malkov A.A., Ishutina Zh.N., Malygin A.A. Phase formation in a nanosize silicon oxide film on the surface of aluminum oxide. *Tech. Phys. Lett.*, 1998, **24** (1), P. 1–3.
[51] Gusarov V.V., Ishutina Zh.N., Malkov A.A., Malygin A.A. Solid-phase reaction of mullite formation in nanosized composite films. *Dokl. Phys. Chem.*, 1997, **357** (1–3), P. 360–363.
[52] Ivanov V.K., Polezhaeva O.S. Synthesis of ultrathin ceria nanoplates. *Rus. J. Inorg. Chem*., 2009, **54** (10), P. 1528–1530.
[53] Čubovä K., Čuba V. Synthesis of inorganic nanoparticles by ionizing radiation – a review. *Radiation Physics and Chemistry*, 2019, **158**, P. 153–164.
[54] Roca A.G., Gutiérrez L., et al. Design strategies for shape-controlled magnetic iron oxide nanoparticles. *Advanced Drug Delivery Reviews*, 2019, **138**, P. 68–104.
[55] Rajeshkumar S., Naik Poonam. Synthesis and biomedical applications of cerium oxide nanoparticles – A Review. *Biotechnology Reports*, 2018, **17**, P. 1–5.
[56] Krl A., Pomastowski P., et al. Zinc oxide nanoparticles: Synthesis, antiseptic activity and toxicity mechanism. *Advances in Colloid and Interface Science*, 2017, **249**, P. 37–52.
[57] Saad W.S., Prud'homme R.K. Principles of nanoparticle formation by flash nanoprecipitation. *Nanotoday*, 2106, **11** (2), P. 212–227.
[58] Calvache-Muñoz J., PradoJorge F.A., Rodríguez-Páez E. Cerium oxide nanoparticles: Synthesis, characterization and tentative mechanism of particle formation. *Colloids and Surfaces A: Physicochemical and Engineering Aspects*, 2017, **529**, P. 146–159.
[59] Byrappa K., Adschiri T. Hydrothermal technology for nanotechnology. *Progress in crystal growth and characterization of materials*, 2007, **53** (2), P. 117–166.
[60] Merzhanov A.G. SHS Process: Combustion Theory and Practice. *Archivum Combustionis*, 1981, **1** (1–2), P. 23–48.
[61] Merzhanov A.G. Theory and Practice of SHS: Worldwide state of the art and the newest results. *Int. J. Self-Prop. High-Temp. Synth.*, 1993, 2 (2), P. 113–158.
[62] Mukasyan A.S., Rogachev A.S. Combustion synthesis: mechanically induced nanostructured materials. *J. Mater. Sci.*, 2017, **52**, P. 11826–11833.
[63] Popkov V.I., Almjasheva O.V., et al. Features of nanosized $YFeO_3$ formation under heat treatment of glycine–nitrate combustion products. *Russ. J. Inorg. Chem.*, 2015, **60** (10), P. 1193–1198.
[64] Popkov V.I., Almjasheva O.V., et al. Crystallization behavior and morphological features of $YFeO_3$ nanocrystallites obtained by glycine-nitrate combustion. *Nanosystems: Physics, Chemistry, Mathematics*, 2015, **6** (6), P. 866–874.
[65] Popkov V.I., Almjasheva O.V., Schmidt M.P., Gusarov V.V. Formation mechanism of nanocrystalline yttrium orthoferrite under heat treatment of the coprecipitated hydroxides. *Russ. J. Gen. Chem.*, 2015. **85** (6), P. 1370–1375.
[66] Lomanova N.A., Tomkovich M.V., Sokolov V.V., Gusarov V.V. Special Features of Formation of Nanocrystalline $BiFeO_3$ via the glycine-nitrate combustion method. *Russ. J. Gen. Chem.*, 2016, **86** (10), P. 2256–2262.
[67] Chen Y., Yang J., et al. Synthesis $YFeO_3$ by salt-assisted solution combustion method and its photocatalytic activity. *J. Ceram. Soc. Japan.*, 2014, **122** (1422), P. 146–150.
[68] Khaliullin Sh.M., Zhuravlev V.D., et al. Solution-combustion synthesis and eletroconductivity of $CaZrO_3$. *Int. J. Self-Prop. High-Temp. Synth.*, 2015, **24** (2), P. 83–88.
[69] Ostroushko A.A., Russkikh O.V. Oxide material synthesis by combustion of organic-inorganic compositions. *Nanosystems: Physics, Chemistry, Mathematics*, 2017, **8** (4), P. 476–502.
[70] Boldyrev V.V. Reactivity of solids. *J. of Thermal Analysis*, 1993, **40** (3), P. 1041–1062.
[71] Kalinin S.V., Vertegel A.A., Oleynikov N.N., Tretyakov Y.D. Kinetics of solid state reactions with fractal reagent. *J. Mater. Synth.*, *Process*, 1998, **6** (5), P. 305–309.
[72] Al'myasheva O.V., Gusarov V.V. Features of the phase formation in the nanocomposites. *Russ. J. Gen. Chem.*, 2010, **80** (3), P. 385–390.
[73] Ashgriz N., Brocklehurst W., Talley D. Mixing mechanisms in a pair of impinging jets. *J. Propul. Power.*, 2001, **17** (3), P. 736.
[74] Handbook of Atomization and Sprays/Ed. N. Ashgriz. Toronto: Springer Science + Business Media, LLC, 2011. Ch. 30., P. 685.

[75] Erkoc E., Fonte C.P., et al. Numerical study of active mixing over a dynamic flow field in a T-jets mixer – Induction of resonance. *Chem. Eng. Res. Design*., 2016, **106**, P. 74.
[76] Ravi Kumar D.V., Prasad B.L.V., Kulkarni A.A. Impinging jet micromixer for flow synthesis of nanocrystalline MgO: Role of mixing/impingement zone. *Ind. Eng. Chem. Res.*, 2013, **52**, P. 17376.
[77] Proskurina O.V., Nogovitsin I.V., et al. Formation of $BiFeO_3$ nanoparticles using impinging jets microreactor. *Russ. J. Gen. Chem.*, 2018, **88** (10), P. 2139–2143.
[78] Proskurina O.V., Abiev R.S., et al. Formation of nanocrystalline $BiFeO_3$ during heat treatment of hydroxides co-precipitated in an impinging-jets microreactor. *Chemical Engineering and Processing – Process Intensification*, 2019, **143**, P. 107598.
[79] Proskurina O.V., Sivtsov E.V., et al. Formation of rhabdophane-structured lanthanum orthophosphate nanoparticles in an impinging-jets microreactor and rheological properties of sols based on them. *Nanosystems: Physics, Chemistry, Mathematics*, 2019, **10** (2), P. 206–214.
[80] Abiev R.S., Almyasheva O.V., Izotova S.G., Gusarov V.V. Synthesis of cobalt ferrite nanoparticles by means of confined impinging-jets reactors. *J. Chem. Tech. App*., 2017, **1** (1), P. 7–13.
[81] Koutzarova T., Kolev S., et al. Microstructural study and size control of iron oxide nanoparticles produced by microemulsion technique. *Phys. Stat. Sol.*, **3** (5), P. 1302–1307.
[82] Ganguli A.K., Ahmad T., Vaidya S., Ahmed J. Microemulsion route to the synthesis of nanoparticles. *Pure Appl. Chem.*, 2008, **80** (11), P. 2451–2477.
[83] Koltsov I., Kimmel G., et al. The new nano-enabled phase map of ZrO_2–Al_2O_3. *Scientific Reports*, 2019, **9**, P. 5540.
[84] Kovalenko A.N., Tugova E.A. Thermodynamics and kinetics of non-autonomous phases formation in nanostructured materials with variable functional properties. *Nanosystems: Physics, Chemistry, Mathematics*, 2018, **9** (5), P. 641–662.
[85] Tauson V.L., Akimov V.V. Effect of crystallite size on solid state miscibility: applications to the pyrite- cattierite system. *Gochimica et Cosmocimica Acta*, 1991, **55** (10), P. 2851–2859.
[86] Emerging materials for energy conversion and storage. Edited by: Cheong K.Y., Impellizzeri G., Amorim Fraga M., 2018, 418 p.
[87] Singh S., Barick K.C., Bahadur D. Functional oxide nanomaterials and nanocomposites for the removal of heavy metals and dyes. *Nanomater. nanotechnol.*, 2013, **3**, 20:2013.
[88] NIST-JANAF Thermochemical Tables. `URL: http://kinetics.nist.gov/janaf/ .`
[89] Iorish V.S, Belov G.V. IVTANTHERMO/WIN – database and software for high temperature chemical processes modeling. *9th Int. Conf. on High Temperature Materials Chemistry: Proceedings*, Pennsylvania (USA), 1997. P. 42.
[90] Aruna S.T., Mukasyan A.S., Combustion synthesis and nanomaterials. *Curr. Opin. Solid State Mater. Sci.*, 2008, **12** (3–4), P. 44–50.
[91] Gabala M.A., Al-Solami F., et al. Auto-combustion synthesis and characterization of perovskite-type $LaFeO_3$ nanocrystals prepared via different routes. *Ceramics International*, 2019, **45** (13), P. 16530–16539.
[92] Karpov O.N., Tomkovich M.V., Tugova E.A. Formation of $Nd_{1-x}Bi_xFeO_3$ nanocrystals under conditions of glycine-nitrate synthesis. *Russ. J. Gen. Chem.*, 2018, **88** (10), P. 2128–2133.
[93] Tugova E., Yastrebov S., Karpov O., Smith R. $NdFeO_3$ nanocrystals under glycine nitrate combustion formation. *J. Cryst. Growth*, 2017, **467**, P. 88–92.
[94] Tugova E.A., Gusarov V.V. Structure peculiarities of nanocrystalline solid solutions in $GdAlO_3$–$GdFeO_3$ system. *Nanosystems: Physics, Chemistry, Mathematics*, 2013, **4** (3), P. 352–356.
[95] Almjasheva O.V., Fedorov B.A., Smirnov A.V., Gusarov V.V. Size, morphology and structure of the particles of zirconia nanopowder obtained under hydrothermal conditions. *Nanosystems: Physics, Chemistry, Mathematics*, 2010, **1** (1), P. 26–36.
[96] Klein S.M., Choi J.H., Pine D.J., Lange F.F. Synthesis of rutile titania powders: Agglomeration, dissolution, and reprecipitation phenomena. *J. Mater. Res.*, 2003, **18** (6), P. 1457–1464.
[97] Krishnankutty-Nair P. Kumar Growth of rutile crystallites during the initial stage of anatase-to-rutile transformation in pure titania and titania-alumina nanocomposites. *Scripta Metallurgica et Materialia*, 1995, **32** (6), P. 873–877.
[98] Vasilevskaia A.K., Popkov V.I., Valeeva A.A., Rempel' A.A. Formation of nonstoichiometric titanium oxides nanoparticles Ti_nO_{2n-1} upon heat-treatments of titanium hydroxide and anatase nanoparticles in a hydrogen flow. *Russ. J. Appl. Chem.*, 2016, **89** (8), P. 1211–1220.
[99] Guang M., Xia Y., et al. Controllable synthesis of transparent dispersions of monodisperse anatase-TiO_2 nanoparticles and nanorods. *Materials Chemistry and Physics*, 2019, **224**, P. 100–106.
[100] Macwan D.P., Dave P.N., Chaturvedi S. A review on nano-TiO_2 sol-gel type syntheses and its applications. *J. Mater. Sci.*, 2011, **46** (11), P. 3669–3686.
[101] Li C.-J., Yang G.-J., Wang Z. Formation of nanostructured TiO_2 by flame spraying with liquid feedstock. *Mater. Lett.*, 2003, **57** (13–14), P. 2130–2134.
[102] Kominami H., Kohno M., Kera Y. Synthesis of brookite-type titanium oxide nano-crystals in organic media. *J. Mater. Chem.*, 2000, **10** (5), P. 1151–1156.
[103] Deng Q., Wei M., et al. Brookite-type TiO_2 nanotubes. *Chem. Commun.*, 2008, **31**, P. 3657–3659.
[104] Zaboeva E.A., Izotova S.G., Popkov V.I. Glycine-nitrate combustion synthesis of $CeFeO_3$-based nanocrystalline powders. *Russ. J. Appl. Chem.*, 2016, **89** (8), P. 1228–1236.
[105] Popkov V.I., Tolstoy V.P., Omarov S.O., Nevedomskiy V.N. Enhancement of acidic-basic properties of silica by modification with CeO_2–Fe_2O_3 nanoparticles via successive ionic layer deposition. *Appl. Surf. Sci.*, 2019, **473**, P. 313–317.
[106] Li L., Pu S., et al. High-purity disperse α-Al_2O_3 nanoparticles synthesized by high-energy ball milling. *Adv. Powder Technol.*, 2018, **29** (9), P. 2194–2203.
[107] Tabesh S., Davar F., Loghman-Estarki M.R. Preparation of γ-Al_2O_3 nanoparticles using modified sol-gel method and its use for the adsorption of lead and cadmium ions. *J. Alloys Comp.*, 2018, **730**, P. 441–449.
[108] Kotlovanova N.E., Matveeva A.N., et al. Formation and Acid–Base Surface Properties of Highly Dispersed η-Al_2O_3 Nanopowders. *Inorg. Mater.*, 2018, **54** (4), P. 392–400.
[109] Kuchina Y.A., Subbotin D.I., et al. Metal ferrites synthesis by AC plasma torch. *J. Phys. Conf. Ser.*, 2018, **1135**, P. 012095.
[110] Dudnik Y.D., Safronov A.A., et al. Plasma ways to obtain ultrafine oxides. *J. Phys. Conf. Ser.*, 2019, **1147**, P. 012127.
[111] Elouafi A., Moubah R., et al. Finite size effects on the magnetocaloric properties around blocking temperature in γ-Fe_2O_3 nanoparticles. *Physica A: Statistical Mechanics and Its Applications*, 2019, **523**, P. 260–267.

[112] Hasan M., Islam Md. F., et al. A soft chemical route to the synthesis of $BiFeO_3$ nanoparticles with enhanced magnetization. *Mat. Res. Bull.*, 2016, **73**, P. 179–186.

[113] Ortiz-Quinonez J.L., Diaz D., et al. Easy synthesis of high-purity $BiFeO_3$ nanoparticles: new insights derived from the structural, optical, and magnetic characterization. *Inorg Chem.*, 2013, **52**, P. 10306–10317.

[114] Park T.-J., Papaefthymiou G.C., et al. Size- dependent magnetic properties of single-crystalline multiferroic $BiFeO_3$ nanoparticles. *Nano Lett*., 2007, **7**, P. 766–772.

[115] Proskurina O.V., Tomkovich M.V., et al. Formation of Nanocrystalline $BiFeO_3$ under Hydrothermal Conditions. *Russ. J. Gen.Chem.*, 2017, **87** (11), P. 2507–2515.

[116] Morales L.A., Sierra-Gallego G., Barrero C.A., Arnache O. Relative recoilless F-factors in $REFeO_3$ (RE = rare-earth La, Pr, Nd and Sm) orthoferrites synthesized by self-combustion method. *Materials Science and Engineering B*, 2016, **211**, P. 94–100.

[117] Luu M.D., Dao N.N., et al. A new perovskite-type $NdFeO_3$ adsorbent: synthesis, characterization, and As(V) adsorption. *Adv. Nat. Sci.: Nanosci. Nanotechnol*., 2016, **7**, P. 025015.

[118] Chanda S., Saha S., Dutta A., Sinha T.P. Raman spectroscopy and dielectric properties of nanoceramic $NdFeO_3$. *Mater. Res. Bull.*, 2013, **48** (4), P. 1688–1693.

[119] Shanker J., Rao G.N., Venkataramana K., Babu D.S. Investigation of structural and electrical properties of $NdFeO_3$ perovskite nanocrystalline. *Phys.Lett. A*, 2018, **382** (40), P. 2974–2977.

[120] Atta N.F., El-Ads E.H., Galal A. Evidence of Core-Shell Formation between $NdFeO_3$ nano-perovskite and ionic liquid crystal and its application in electrochemical sensing of metoclopramide. *J. Electrochem. Soc.*, 2016, **163** (7), P. B325–B334.

[121] Atta N.F., Galal A., Ali S.M. The Effect of the Lanthanide Ion-Type in $LnFeO_3$ on the Catalytic Activity for the Hydrogen Evolution in Acidic Medium. *Int. J. Electrochem. Sci.*, 2014, **9**, P. 2132–2148.

[122] Atta N.F., Binsabt M.H., El-Ads E.H., Galal A. Synthesis of neodymium-iron nanoperovskite for sensing applications of an antiallergic drug. *Turk. J. Chem.*, 2017, **41** (4), P. 476–492.

[123] Ho T.G., Ha T.D., et al. Nanosized perovskite oxide $NdFeO_3$ as material for a carbon-monoxide catalytic gas sensor. *Adv. Nat. Sci: Nanosci. Nanotechnol.*, 2011, **2**, P. 015012.

[124] Yousefi M., Soradi Zeid S., Khorasani-Motlagh M. Synthesis and characterization of nano-structured perovskite type neodymium orthoferrite $NdFeO_3$. *Curr. Chem. Lett.*, 2017, **6** (1), P. 23–30.

[125] Hao Y.J., Li B., Liu R.H., Li F.T. Synthesis of $NdFeO_3$ perovskites in a reverse microemulsion and its visible light photocatalytic activity. *Adv. Mater. Res.*, 2011, **282–283**, P. 593–596.

[126] Popkov V.I., Almjasheva O.V. Yttrium orthoferrite $YFeO_3$ nanopowders formation under glycine-nitrate combustion conditions. *Russ. J. Appl. Chem.*, 2014, **87** (2), P. 167–171.

[127] Popkov V.I., Almjasheva O.V., et al. Magnetic properties of $YFeO_3$ nanocrystals obtained by different soft-chemical methods. *J. Mater. Sci.: Mater. Electron.*, 2017, **28** (10), P. 7163–7170.

[128] Popkov V.I., Almjasheva O.V., et al. Effect of spatial constraints on the phase evolution of $YFeO_3$-based nanopowders under heat treatment of glycine-nitrate combustion products. *Ceram. Int.*, 2018, **44** (17), P. 20906–20912.

[129] Popkov V.I., Tugova E.A., Bachina A.K., Almyasheva O.V. The formation of nanocrystalline orthoferrites of rare-earth elements $XFeO_3$ (X = Y, La, Gd) via heat treatment of coprecipitated hydroxides. *Russ. J. Gen. Chem.*, 2017, **87** (11), P. 2516–2524.

[130] Gimaztdinova M.M., Tugova E.A., Tomkovich M.V., Popkov V.I. Glycine-nitrate combustion synthesis of $GdFeO_3$ nanocrystals. *Condens. Matter and Interphases*, 2016, **18** (3), P. 422–431.

[131] Martinson K.D., Kondrashkova I.S., Popkov V.I. Synthesis of $EuFeO_3$ nanocrystals by glycine-nitrate combustion method. *Russ. J. Appl. Chem.*, 2017, **90** (8), P. 1214–1218.

[132] Kondrashkova I.S., Martinson K.D., Zakharova N.V., Popkov V.I. Synthesis of nanocrystalline $HoFeO_3$ photocatalyst via heat treatment of products of glycine-nitrate combustion. *Russ. J. Gen. Chem.*, 2018, **88** (12), P. 2465–2471.

[133] Zhi-hui C., Jun-fu Q., et al. Preparation of $Bi_4Ti_3O_{12}$ nanopower by azeotropic co-precipitation and dielectric properties of the sintered ceramic. *Ceram. Intern.*, 2010, **36** (1), P. 241–244.

[134] Chen D., Jiao X. Hydrothermal synthesis and characterization of Bi4Ti3O12 powders from different precursors. *Materials Research Bulletin*, 2001, **36**(1–2), P. 355–363.

[135] Al-Amani U., Sreekantan S., Fauzi A.M.N., Khairunisak A.R., Warapong K. Soft combustion technique: Solution combustion synthesis and low-temperature combustion synthesis; to prepare $Bi_4Ti_3O_{12}$ powders and bulk ceramics. Science of Sintering, 2012, **44** (2), P. 211–221.

[136] Zhang H., Ke H., et al. Crystallisation process of $Bi_5Ti_3FeO_{15}$ multiferroic nanoparticles synthesized by a sol–gel method. *J. Sol-Gel Sci. Technol.*, 2018, **85** (1), P. 132–139.

[137] Gautam A., Singh K., et al. Crystal structure and magnetic property of Nd doped $BiFeO_3$ nanocrytallites. *Mater. Lett.*, 2011, **65**, P. 591–594.

[138] Mishra R.K., Pradhan D.K., Choudhary R.N.P., Banerjee A. Dipolar and magnetic ordering in Nd-modified $BiFeO_3$ nanoceramics. *J. Magn. Magnetic Mater.*, 2008, **320**, P. 2602–2607.

[139] Almjasheva O.V., Smirnov A.V., et al. Structural features of ZrO_2–Y_2O_3 and ZrO_2–Gd_2O_3 nanoparticles formed under hydrothermal conditions. Russ. *J. Gen. Chem.*, 2014, **84** (5), P. 804–809.

[140] Gusarov V.V., Malkov A.A., Malygin A.A., Suvorov V.A. Formations of aluminum titanate in compositions with a high level of spatial and structural conjugation of components. *Russ. J. Gen. Chem.*, 1994, **64** (4), P. 554.